NANO LETTERS

2009
Vol. 9, No. 12
4191-4197

Controlling Nanogap Quantum Dot Photoconductivity through Optoelectronic Trap Manipulation

Lauren J. Willis,† Jessamyn A. Fairfield,† Tali Dadosh,† Michael D. Fischbein, and Marija Drndic*

Department of Physics and Astronomy, University of Pennsylvania, Philadelphia, Pennsylvania 19104

Received July 27, 2009; Revised Manuscript Received September 18, 2009

ABSTRACT

Nanoscale devices are being extensively studied for their tunable electronic and optical properties, but the influence of impurities and defects is amplified at these length scales and can lead to poorly understood variations in characteristics of semiconducting materials. By performing a large ensemble of photoconductivity measurements in nanogaps bridged by core-shell CdSe/ZnS semiconductor nanocrystals, we discover optoelectronic methods for affecting solid-state charge trap populations. We introduce a model that unifies previous work and transforms the problem of irreproducibility in nanocrystal electronic properties into a reproducible and robust photocurrent response due to trap state manipulation. Because traps dominate many physical processes, these findings may lead to improved performance and device tunability for various nanoscale applications through the control and optimization of impurities and defects.

One of the grand challenges of nanoscale systems is to control local fluctuations and disorder. As size decreases, the importance of individual defects and impurities grows, and they can cause unpredictable and undesired changes in behavior. Charge traps are ubiquitous and can affect a variety of systems such as electronic states in graphene,[1] charge transport in carbon nanotubes,[2] photoluminescence intermittency in semiconducting nanocrystals and nanorods,[3,4] and telegraph noise in resistance.[5] Local fluctuations often act as "hidden variables" that foil attempts at quantitative property measurement and interpretation. Hence, the discovery of ways to detect and control trap behavior will hasten progress in the field of nanoscience.

Nanocrystal quantum dots are being studied for a broad range of optoelectronic applications, including the realization of tunable and efficient photodetectors,[6−10] solar cells,[11,12] and light emitters.[13] CdSe/ZnS core-shell nanocrystals are particularly interesting because of their high quantum yield, large bandgap tunability across the visible spectrum, and well-established synthesis protocols.[14−16] Quantum dot arrays are light-sensitive artificial solids that serve as flexible model systems for the study of basic transport phenomena, arising from the interplay between the recombination-rate limited and thermally activated charge transport mechanisms.[10,17−19] Prior studies have considered the presence of traps in these systems but were not able to quantify or control them.

Here we demonstrate a robust and reproducible procedure for controlling the trap population in nanocrystal nanogap devices and show that qualitatively different photocurrent behaviors can be produced depending on how traps are initialized prior to a measurement. Electric field-induced population and optically induced depopulation of traps can reverse the temperature dependence of the photoconductivity. We present a model that explains the role of traps and the importance of measurement sequence. Our method for dynamically controlling trap populations achieves optimized photodetector sensitivity at low or high temperatures for light sources, photovoltaics, electronics, and other applications. Moreover, we show that a range of temperature-dependent behaviors previously attributed to material differences are reproducible in a single device and provide a possible explanation for contradictory reports of the temperature dependence of photoconductivity in the literature.[10,17,19−22] These results carry implications for past and future experiments and may inspire analogous procedures for trap manipulation in other systems.

Figure 1a shows the schematic representation of the photodetector device based on nanocrystals in a nanogap electrode geometry. Electrodes made of 3 nm of nickel and 30 nm of gold, separated by only 20−30 nm, ∼4 nanocrystal diameters, are patterned using electron beam lithography on a silicon nitride (Si_3N_4) membrane.[23] The membrane is compatible with high-resolution structural characterization using transmission electron microscopy (TEM), which allows

* To whom correspondence should be addressed. E-mail: drndic@physics.upenn.edu. Phone: 215-898-5810. Fax: 215-898-2010.
† These authors contributed equally to this work.

10.1021/nl9024209 CCC: $40.75
Published on Web 10/14/2009

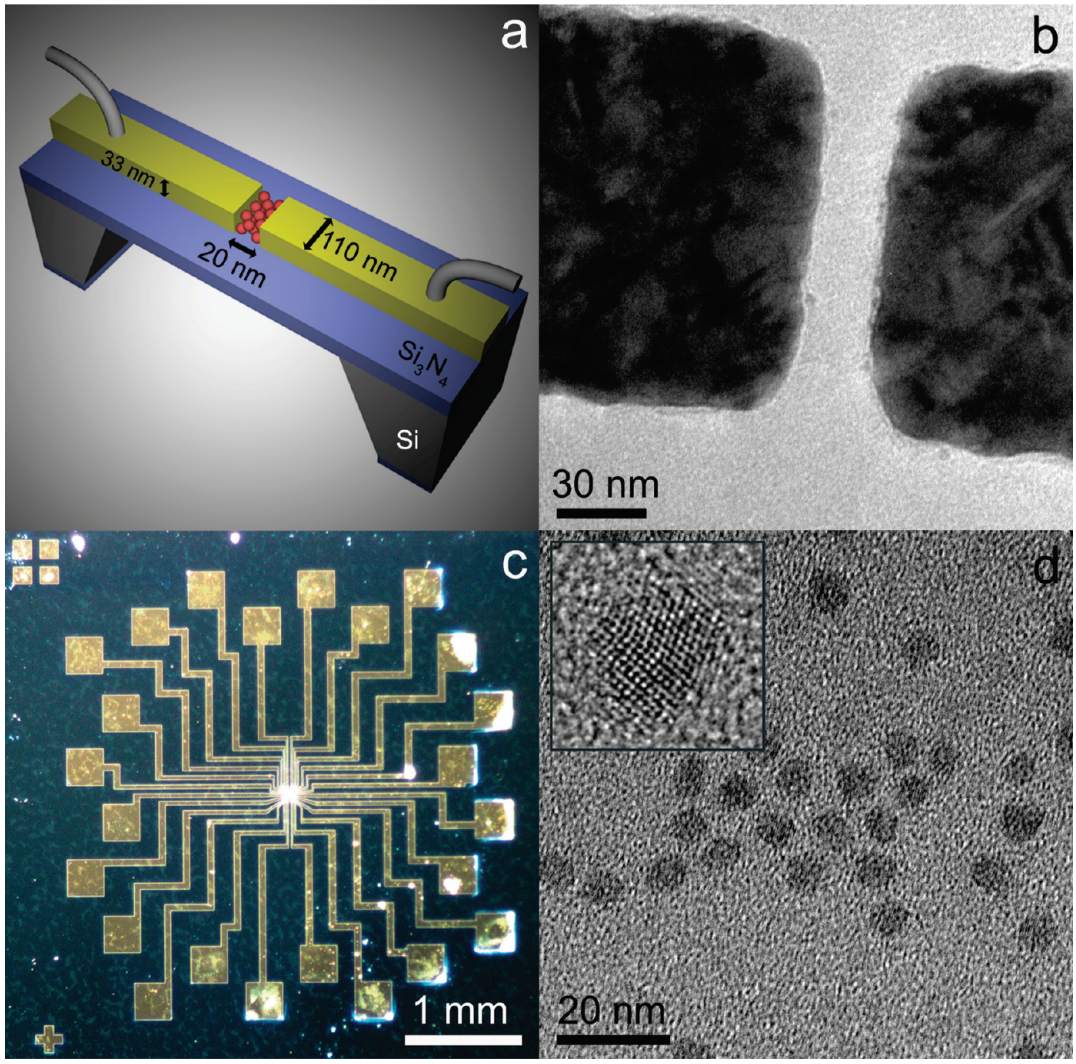

Figure 1. (a) Schematic of the photodetector nanogap device. Metal electrodes (3 nm of Ni and 30 nm of Au) separated by 20 to 30 nm are patterned on top of a 40 nm Si_3N_4 membrane that is supported by a Si wafer. Nanocrystals are deposited on the substrate and electrodes. (b) TEM image of the Ni/Au electrodes separated by 20 nm prior to nanocrystal deposition. (c) Optical image of the device with 12 electrode pairs. (d) TEM image of CdSe/ZnS nanocrystals with an average size of 5.2 ± 0.6 nm. Inset: Zoomed-in TEM image of a single nanocrystal.

us to confirm that the nanogaps did not have any metallic debris, as shown in Figure 1b. An optical image of lithographic features on a typical device is shown in Figure 1c. For more details on device fabrication, please see Supporting Information Section 1. One advantage of nanoscale gaps is that the application of relatively small voltages yields high electric fields in the gap area. For a 20 nm gap with a bias voltage of 2 V, the field strength experienced in the 2000 nm^2 of active area is 10^8 V/m. The active area of these photodetectors in comparison to previous literature[17−19] is decreased by 6 orders of magnitude in area and decreased in gap size by 2 orders of magnitude.

We used Sigma-Aldrich CdSe/ZnS core-shell nanocrystals, as shown in Figure 1d, which had an average diameter of 5.2 nm, and a shell thickness of ∼0.2 nm or ∼1 monolayer. Before any treatment, the nanocrystals have a primary absorption peak at 610 nm and emit at 640 nm. The nanocrystals were capped with a mixture of hexadecylamine and trioctylphosphine ligands to prevent aggregation and passivate surface traps. Five microliters of the nanocrystal solution were dropcast onto the chip and allowed to dry, forming a multilayer nanocrystal film on the surface. For more characterization of the nanocrystals used, see Supporting Figures S1−S3.

Electrical measurements were performed in either a modified Janis VPF-700 or ST-100H cryostat operated at $\sim 5 \times 10^{-7}$ torr. Nanogaps were wire bonded to a ceramic chip carrier thermally coupled to a copper cold finger and fitted into a Macor socket electrically addressed by silver-soldered wires making it compatible with high temperature operation, which coupled the source and drain pins to two independent BNC breakout boxes. Voltages were applied with a Yokogawa 7651 programmable DC source; current signals were amplified and filtered by a Keithley 428 current amplifier and measured with an Agilent 34401A digital multimeter. For all measurements at fixed laser intensity, the $I-V$ characteristics for each device were measured by sweeping the voltage across the nanogap from 0 V to 2 V to

−2 V and back to 0 V with a typical cycle taking 200 s. This gives a maximum voltage drop per nanocrystal of 0.5 V. Prior to nanocrystal deposition and after TEM inspection, the bare devices were cleaned with an O_2 plasma, then the conductance and photoresponse of the bare devices were tested. The dark current of devices was measured by performing an $I-V$ sweep with the nanogap in the dark, and photocurrent was measured by performing an $I-V$ sweep while the nanogap was illuminated by a continuous wave 532 nm diode laser. In each measurement set, we measured at room temperature the dark current of all devices on a chip, and then the photocurrent of the same devices; the device was then cooled with either liquid nitrogen or liquid helium, and both dark current and photocurrent were measured again at low temperature. Changing measurement order, for example, performing low-temperature measurements first and room-temperature measurements second, did not affect current characteristics.

The samples were annealed in situ because annealing has been shown to increase photocurrent in nanocrystal solids[17−19,22] by reducing interparticle separation and lowering tunneling barriers. We detected photocurrent in 17 nanogaps, and no dark current signal above the maximum noise floor of ∼0.03 pA at 295 K and ∼0.15 pA at 78 K in 70% of devices after annealing up to 573 K. From TEM imaging we confirmed that nanogaps did not have any metallic debris that could contribute to the dark current, and this was consistent with our subsequent $I-V$ characterization of the nanogaps. More importantly, all of our photocurrent is primary, which means it is a result of direct exciton generation in the nanocrystals and that there is no measurable charge injection from the metal electrodes into the nanocrystal film.[21] For more details about the effect of annealing on photocurrent and dark current measurements, see Supporting Information Section 3 and Figures S4−S6.

Figure 2 shows the $I-V$ response under 532 nm illumination at different temperatures of two different nanogaps. The photocurrent is well described by a second-order polynomial in voltage. Measurements at other wavelengths show consistent behavior once temperature-dependent absorption shifts are accounted for; see Supporting Information Figure S7 for $I-V$ characteristics obtained using different illumination wavelengths. Over all measured devices, the initial room temperature photocurrent was in the range of 0.1 to 50 pA with a mean value of ∼5 pA, and the initial low temperature photocurrent was in the range of 0.1 to 240 pA, with a mean value of ∼30 pA. A histogram of photocurrent values is shown in Supporting Information Figure S8. The large variation in measured photocurrent is probably due to the small number of nanocrystals in the nanogap; thus the variations in each individual nanocrystal are not averaged out. Additionally, film thickness within the nanogap and the energy barrier at the contacts between the nanocrystals and the electrodes may vary. Transport through the nanocrystals inside the gap dominates the photocurrent, while nanocrystals outside the gap region have a negligible contribution.[6] Although more than just the gap area is illuminated, outside the gap, the high barrier to interparticle transport and the low field prevent significant contribution to photocurrent. See Supporting Information Figures S9 and S10 for optical and TEM images of measured nanogaps.

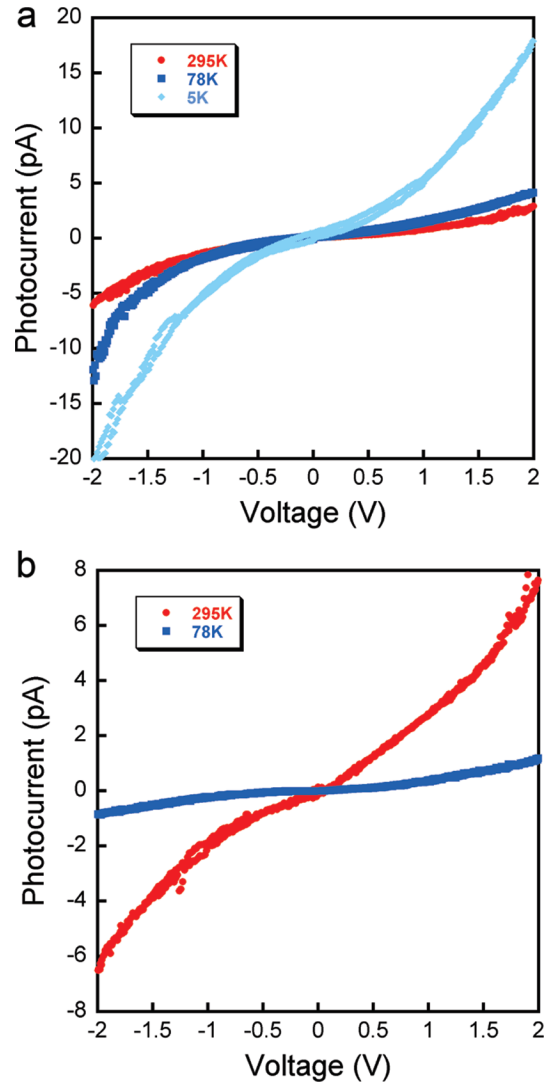

Figure 2. Photocurrent versus voltage curves at 5 K (light blue), 78 K (dark blue), and 295 K (red) for CdSe/ZnS nanocrystals in devices where the low temperature photocurrent is higher (a) or lower (b) than the room temperature photocurrent.

We observed that the magnitude of the measured photocurrent depends on the recent illumination history of the device. Even more strikingly, some nanogaps showed photocurrent that was higher at 295 K than at lower temperatures, while other nanogaps on the same chip and under equivalent conditions showed the opposite. Moreover, if the nanocrystals were illuminated overnight and voltage was applied (hereafter referred to as a laser voltage treatment), the low-temperature photocurrent was enhanced, whereas if the nanocrystals were left in darkness overnight and voltage was applied (hereafter referred to as a dark voltage treatment), the low-temperature photocurrent was suppressed. If voltage was not applied while the sample was left in darkness overnight, the photocurrent magnitude returned to its initial value. This trend was repeatable over a measurement period of several months. The photocurrent at 295 K followed the same trend as the low-temperature photocurrent in ∼75% of devices,

but the effect was smaller (~10−30% of the photocurrent change at 78 K).

To best quantify the photocurrent increase or decrease with temperature, T, it is convenient to define the relative photocurrent ratio $R = I_{78K}/I_{295K}$, of the low-temperature photocurrent, I_{78K}, and the room-temperature photocurrent, I_{295K}. This is analogous to the relative resistance ratio between the low- and room-temperature resistance in metals, commonly used as a criterion of metal purity; if the photoconduction in nanogaps were ohmic, resistance would be well-defined, and then R would be the same as that defined for metals. Each ratio R was calculated for one cool-down cycle of measurements taken in a single day. The relative photocurrent ratio has two distinguishable regimes; if $R < 1$, this means that the photocurrent increased with T, and if $R > 1$, the photocurrent decreased with T. In the discussion below, I_{78K} and I_{295K} were calculated as averages of photocurrent magnitudes for the maximum electric field applied across the nanogaps, corresponding to voltages −2 and 2 V. The following conclusions hold qualitatively for other voltages and also apply independently of annealing temperature. Examples of nanogaps with $R = I_{78K}/I_{295K}$ smaller or greater than 1 are shown in Figure 2a ($R = 2.2$) and Figure 2b ($R = 0.1$). Out of the 17 nanogaps, 15 initially showed $R > 1$ and 2 showed $R < 1$. A histogram of R values for 532 nm illumination and a comparison of R values for both 532 and 650 nm illumination are given in Supporting Information Figures S11 and S12. As measurements progressed, illumination history was observed to affect this ratio, so that R could be switched from less than 1 to greater than 1 or vice versa in a single nanogap. A sample table of the change in relative photocurrent ratios after laser and dark voltage treatments is given in Supporting Information Table S1.

Figure 3 shows a histogram of the change in R from $R_{initial}$ to R_{final} from 70 measurements over all devices after laser and dark voltage treatments. We use a logarithm transformation to write the change in R on the x-axis as $\ln(R_{final}/R_{initial})$. This manner of representing the change in R is informative because $\ln(R_{final}/R_{initial}) = -\ln(R_{initial}/R_{final})$, meaning that an increase or decrease of R by the same factor is represented on this scale symmetrically around zero; $\ln(R_{final}/R_{initial}) = 0$ means that R does not change. There are two distinct distributions in this histogram, showing that device behavior after a laser and dark voltage treatment is clearly separated. The laser voltage treatment increases the ratio by an average factor of 2.2, meaning that $R_{final} > R_{initial}$. The dark voltage treatment decreases the ratio by an average factor of 10, meaning that $R_{final} < R_{initial}$. We have also observed this effect in a large gap with an active area of ~109 μm^2 (~43.6 × 2.5 μm), implying that this effect is independent of device size.

This demonstrated change in ratio R with laser or dark voltage treatments shows that the temperature dependence of conductivity is controlled by the measurement protocol. Consequently, all such measurements on nanocrystal arrays must be framed in the context of the sample measurement history in order to be properly interpreted. This consideration may explain apparent discrepancies in the reported temperature dependence of observed photocurrent.[10,17,19−22] As we will demonstrate, localized charge carriers in the nanogap can measurably affect the temperature dependence of photoconductivity. The manipulation of trap states by optically stimulated emptying or voltage induced populating can then be used to control device performance.

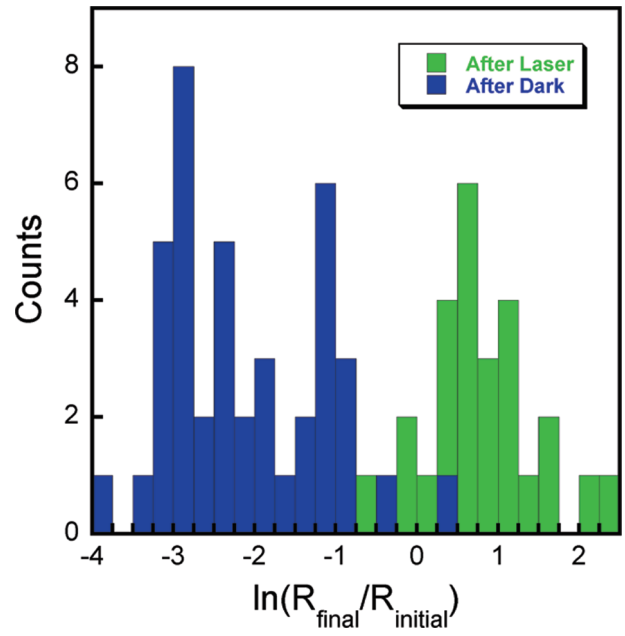

Figure 3. Histogram of the change in the final ratio with respect to the initial ratio, $R_{final}/R_{initial}$, on a logarithmic scale with over 70 measurements including laser voltage treatments (green) and dark voltage treatments (blue). An increase or decrease of R by the same factor is represented on this logarithmic scale symmetrically around zero. Two distinct distributions clearly show that R increases after a laser voltage treatment and decreases after a dark voltage treatment on average 2.2 and 10 times, respectively.

To understand the underlying mechanism, we must first look at the energy levels through which the charge carriers travel. Figure 4a shows energy levels for the electrodes with a single nanocrystal between them; the shortest charge carrier path in our devices includes four nanocrystals. The carrier tunneling between nanocrystals can be lost by recombining with other oppositely charged carriers through radiative or nonradiative recombination, which usually corresponds to free recombination or recombining with trapped carriers at recombination centers, respectively. The primary photocurrent in a semiconductor is given by

$$I(E, T) = eFG \tag{1}$$

where e is the charge of an electron, F is the exciton generation rate, and G is the number of free charge carriers created that pass between the electrodes for each photon absorbed, which is also called the photoconductive gain.[18,19,24] F is defined by[19]

$$F = \Phi a \eta(E, T) \tag{2}$$

where Φ is the excitation flux, a is the film absorption, and $\eta(E,T)$ is the field-dependent exciton separation efficiency.

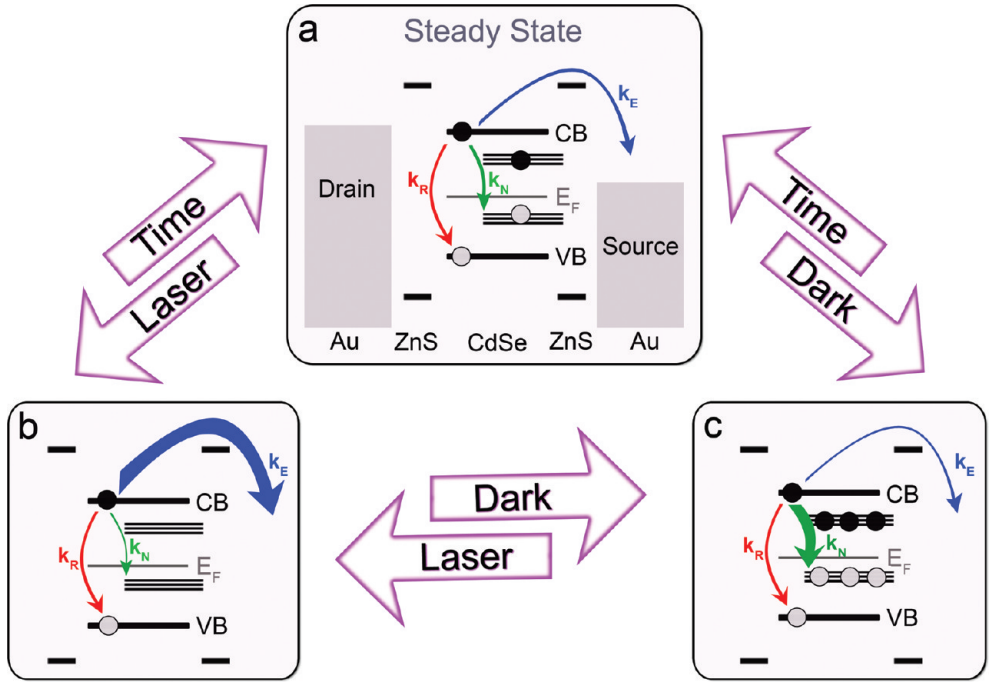

Figure 4. (a) The energy level diagram for a steady state CdSe/ZnS core-shell nanocrystal between two gold electrodes. Trap states above the Fermi energy, E_F, act as electron traps, whereas trap states below E_F act as hole traps. An exciton is created by illumination of the sample, and it can either recombine radiatively with rate k_R, recombine nonradiatively via the trap states with rate k_N, or tunnel away from the nanocrystal at a rate k_E related to the applied field E. (b) After applying laser voltage treatment, the traps are emptied which enhances k_E and suppresses k_N. (c) After applying dark voltage treatment, the traps are filled, which suppresses k_E and enhances k_N. Over a few days of waiting time, trap populations return to their steady state value, which also returns k_E and k_N to their steady state values. Hole processes are affected by the treatments in the same way, but are not shown.

$\eta(E,T)$ is defined in terms of the relevant rates that affect exciton recombination and transport

$$\eta(E,T) = \frac{k_E(E,T)}{k_E(E,T) + k_R(T) + k_N(T)} \quad (3)$$

where $k_E(E,T)$ is the field-dependent rate of charge carriers escaping to neighboring nanocrystals or electrodes, $k_R(T)$ is the rate of charge carriers radiatively recombining, and $k_N(T)$ is the rate of charge carriers nonradiatively recombining.[24]

The tunable temperature dependence of the observed photocurrent can be explained by the relative magnitudes of the rates $k_R(T)$, $k_N(T)$, and $k_E(E,T)$ involved, shown in Figure 4a, and their temperature dependence. $k_R(T)$ increases with increasing temperature because thermal energy magnifies the probability of free charge carriers to recombine, causing photocurrent to decrease with increasing temperature.[25] $k_N(T)$ decreases with increasing temperature, since at high temperature, less nonradiative recombination occurs because charge carriers easily escape from traps with thermal energy, which causes photocurrent to increase with increasing temperature.[24] The contribution from both radiative recombination and the number of traps is constant over these measurements and fixed for a given sample, but the contribution from trap states depends on trap population, which can be adjusted by laser and dark voltage treatments.

Before any treatment, the system has a number of occupied trap states that is defined as the steady state, as in Figure 4a. The laser voltage treatment creates many charge carriers that recombine with carriers in trap states, causing traps that are occupied in steady state to be emptied, as in Figure 4b; this effect of optically stimulated trap emptying in our nanogaps is similar to an analogous phenomenon well documented in the semiconductor literature.[24] The laser voltage treatment eliminates many charge carriers, even in energetically favorable traps, and fewer charge carriers recombine with trapped charges. This increases photocurrent temporarily, but over a few days of waiting time, the trap occupancy returns to its steady state value, as energetically favorable traps are repopulated, causing photocurrent to return to a steady state value as well. Conversely, the dark voltage treatment repeatedly sweeps the voltage, increasing the population of charge carriers in the traps, as in Figure 4c. Thus, after dark voltage treatment even energetically unfavorable traps are populated; the populated traps capture more carriers and cause them to recombine, temporarily decreasing photocurrent. Over a few days of waiting time the trap occupancy returns to its steady state value, as charge carriers in some traps escape using thermal energy, causing photocurrent to return to a steady state value as well. To summarize, by applying the laser and dark voltage treatments, the trap population is modified, which allows tuning of the photocurrent response; this has a greater effect at low temperature because traps can be emptied using the larger thermal energy at room temperature. Relevant processes for photogenerated electrons in the conduction band are shown in detail in Figure 4. The photocurrent temperature dependence can be tuned

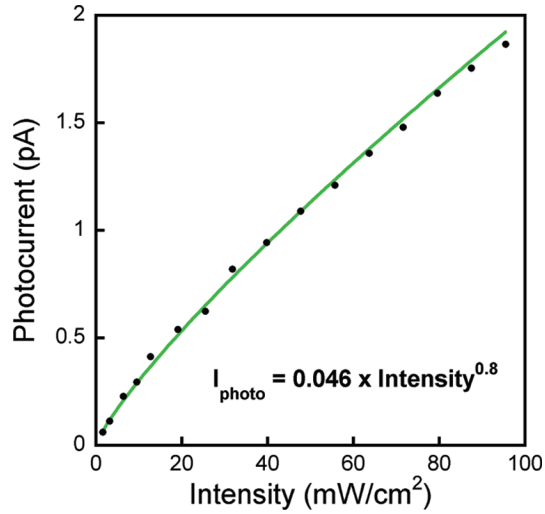

Figure 5. Photocurrent as a function of illumination intensity for 532 nm laser excitation measured at 3×10^7 V/m at 295 K. The green line is a power law fit to the data with an exponent of 0.8.

using these effects, and the resultant adjustability is robust even when other variables are changed.

Measuring photocurrent dependence on laser intensity at a fixed wavelength also supports the trap-based model in explaining the adjustable photocurrent dependence on temperature. While initial photoconductivity measurements were taken with a fixed illumination intensity of ~65 mW/cm^2, intensity was later varied between 1.6 to 120 mW/cm^2 at both 78 and 295 K. As illumination intensity was varied, the current was measured at a constant voltage of 1 V, which corresponds to 3×10^5 V/cm. The laser and dark voltage treatments had little effect on the intensity dependence at 295 K, but had a greater effect at 78 K. The treatments can result in an inversion of the temperature dependence of the photocurrent for a wide range of intensities; see Supporting Figure S13.

At 295 K, the intensity dependence of the photocurrent always followed a power law, $I_{photo} \propto \text{Intensity}^{\alpha}$, where $\alpha = 0.82 \pm 0.02$ over seven measurements, as shown in Figure 5. This is consistent with previous room temperature measurements on large arrays of core-shell nanocrystals yielding the same α value.[19] Intensity dependence of the photocurrent at 78 K gives $\alpha = 0.96 \pm 0.02$ in agreement with the linear response at low temperature reported in the literature.[20] The specific value of α helps reveal the type of carrier dynamics present.

To understand the power law fit, it is instructive to examine the rate equation for n, the density of free electrons[18,24]

$$\frac{dn}{dt} = F - C(n + n_{trap})n \tag{4}$$

Here, C is the probability of an electron to be captured, and n_{trap} is the density of trapped electrons. $n + n_{trap}$ represents the density of holes in the system which can recombine with free electrons, assuming a neutral nanocrystal. For a steady state system, $(dn/dt) = 0$ and we can rewrite F as

$$F \propto (n_{trap} + n)n \tag{5}$$

Substituting eq 2 into eq 5, we can write

$$\Phi \propto \frac{(n_{trap} + n)n}{a\eta} \tag{6}$$

For $n_{trap} \gg n$, $\Phi \propto n$, but for $n_{trap} \ll n$, $\Phi \propto n^2$. Since $n \propto I_{photo}$, this means that for $n_{trap} \gg n$, $I_{photo} \propto \Phi$, but for $n_{trap} \ll n$, $I_{photo} \propto \Phi^{0.5}$. Thus, $\alpha = 1$ implies monomolecular (first-order) carrier dynamics, whereas $\alpha = 0.5$ implies bimolecular (second-order) carrier dynamics.[24] First-order kinetics dominate when the material has many recombination centers, such as deep hole traps, and when the material has a lower free electron concentration than in the bulk, as is the case in nanocrystals where the presence of surface traps is likely.[20] Contributions of surface and deep traps, which are only partially passivated by the shell and ligands, can cause a deviation of the photocurrent dependence on intensity from the expected dependence in a bulk solid, where bimolecular recombination would dominate giving $\alpha = 0.5$. Our measured exponent $\alpha = 0.8$ at room temperature implies that we observe a combination of first and second order recombination dynamics. However, at low temperature we measured an exponent $\alpha = 1$, implying that we observe first-order recombination dynamics. The variation in the fitting exponent sheds light on the difference of recombination center density at each temperature, which supports our proposed model shown in Figure 4 and encompasses reported intensity dependence.[19,20,24]

In conclusion, we have created nanogap devices with CdSe/ZnS core-shell nanocrystals in the gap region; after annealing, these devices can be operated as photodetectors with tunable photoconductivity. We investigated the temperature dependence of photocurrent and found that it depends on the illumination history of the device. Recent laser illumination causes optically induced trap emptying and higher low-temperature photocurrent, while recent voltage cycling in the dark causes electric field induced trap population and lower low-temperature photocurrent. This can resolve existing discrepancies in the literature, demonstrating the difficulty in defining temperature dependence of photoconductivity for semiconducting nanocrystal systems. Additional research in this area could include investigation of trap depopulation time scales, dynamic response, dependence on nanocrystal material or size, and the optimization of treatment parameters. We find our controllable photocurrent temperature dependence to be robust over multiple wavelengths and intensities of laser excitation and suggest a route toward achieving maximal photodetector response at different temperatures. This approach of tuning the photocurrent response via trap population can be useful for nanocrystal device applications, such as sensors, solar cells, and light emitters, as well as aiding in the study of carrier dynamics and energy levels in nanoscale materials.

Acknowledgment. We thank Professor Jay Kikkawa for very helpful discussions. We also thank Professor Catherine

Crouch and Dr. Chris Merchant for useful comments on the manuscript. This work was supported by the DARPA Young Investigator Award HR011-08-1-0031 and partially by ONR (YIP N000140410489) and NSF (NSF Career Award DMR-0449533, NSF MRSEC DMR05-20020, and NSF NSEC DMR-0425780). L.W. acknowledges funding from the NSF-IGERT program (Grant DGE-0221664) and T.D. from the Israel Science Foundation (Bikura postdoctoral fellowship).

Supporting Information Available: Details of device fabrication; nanocrystal characterization, which includes TEM images, a histogram of nanocrystal size, and absorption and emission spectra; additional annealing characterization; dark current $I-V$ plots and Arrhenius fits; $I-V$ curves for different wavelengths of illumination; histograms of photocurrent values at 2 V under 532 nm illumination; optical and TEM images of a chip after nanocrystal deposition, annealing, and measurement; a histogram of I_{78K}/I_{295K} under 532 nm illumination, a histogram of I_{78K}/I_{295K} comparing the effects of using 532 and 650 nm illumination, and a table of changing relative photocurrent ratio; and photocurrent temperature inversion plots. This material is available free of charge via the Internet at http://pubs.acs.org.

References

(1) Tachikawa, H.; Nagoya, Y.; Kawabata, H. A Density Functional Theory Study of Ground and Low-Lying Excited Electronic States in Defective Graphenes *J. Chem. Theory Comput.,* in press.
(2) Tersoff, J. Low-Frequency Noise in Nanoscale Ballistic Transistors. *Nano Lett.* **2007**, *7*, 194.
(3) Cichos, F.; von Borczyskowski, C.; Orrit, M. Power-law intermittency of single emitters. *Curr. Opin. Colloid Interface Sci.* **2007**, *12*, 272.
(4) Querner, C.; Wang, S.; Healy, K.; Fairfield, J. A.; Fischbein, M. A.; Drndic, M. Fluorescence Dynamics of Semiconductor Nanorod Clusters Studied by Correlated Atomic Force, Transmission Electron, and Fluorescence Microscopy. *J. Phys. Chem. C* **2008**, *112*, 19945.
(5) Ralls, K. S.; Skocpol, W. J.; Jackel, L. D.; Howard, R. E.; Fetter, L. A.; Epworth, R. W.; Tennant, D. M. Discrete Resistance Switching in Submicrometer Silicon Inversion Layers: Individual Interface Traps and Low-Frequency (1f?) Noise. *Phys. Rev. Lett.* **1984**, *52*, 228.
(6) Hegg, M.; Lin, L. Y. Near-field photodetection with high spatial resolution by nanocrystal quantum dots. *Opt. Express* **2007**, *15*, 17163.
(7) Konstantatos, G.; Howard, I.; Fischer, A.; Hoogland, S.; Clifford, J.; Klem, E.; Levina, L.; Sargent, E. H. Ultrasensitive solution-cast quantum dot photodetectors. *Nature* **2006**, *442*, 180.
(8) Weiss, E. A.; Chiechi, R. C.; Geyer, S. M.; Porter, V. J.; Bell, D. C.; Bawendi, M. G.; Whitesides, G. M. Size-dependent charge collection in junctions containing single-size and multi-size arrays of colloidal CdSe quantum dots. *J. Am. Chem. Soc.* **2008**, *130*, 74.
(9) Osedach, T. P.; Geyer, S. M.; Ho, J. C.; Arango, A. C.; Bawendi, M. G.; Bulovic, V. Lateral heterojunction photodetector consisting of molecular organic and colloidal quantum dot thin films. *Appl. Phys. Lett.* **2009**, *94*, 043307.
(10) Ginger, D. S.; Greenham, N. C. Photoinduced electron transfer from conjugated polymers to CdSe nanocrystals. *Phys. Rev. B* **1999**, *59*, 10622.
(11) Gur, I.; Fromer, N. A.; Geier, M. L.; Alivisatos, A. P. Air-stable all-inorganic nanocrystal solar cells processed from solution. *Science* **2005**, *310*, 462.
(12) Milliron, D. J.; Gur, I.; Alivisatos, A. P. Hybrid organic - Nanocrystal solar cells. *MRS Bull.* **2005**, *30*, 41.
(13) Snee, P. T.; Chan, Y. H.; Nocera, D. G.; Bawendi, M. G. Whispering-gallery-mode lasing from a semiconductor nanocrystal/microsphere resonator composite. *Adv. Mater.* **2005**, *17*, 1131.
(14) Dabbousi, B. O.; Rodriguez-Viejo, J.; Mikulec, F. V.; Heine, J. R.; Mattoussi, H.; Ober, R.; Jensen, K. F.; Bawendi, M. G. (CdSe)ZnS core-shell Quantum Dots: Synthesis and Characterization of a Size Series of Highly Luminescent Nanocrystallites. *J. Phys. Chem. B* **1997**, *101*, 9463.
(15) Hines, M. A.; Guyot-Sionnest, P. Synthesis and Characterization of Strongly Luminescing ZnS-Capped CdSe Nanocrystals. *J. Phys. Chem.* **1996**, *100*, 468.
(16) Murray, C. B.; Norris, D. J.; Bawendi, M. G. Synthesis and characterization of nearly monodisperse CdE (E = sulfur, selenium, tellurium) semiconductor nanocrystallites. *J. Am. Chem. Soc.* **1993**, *115*, 8706.
(17) Drndic, M.; Jarosz, M. V.; Morgan, N. Y.; Kastner, M. A.; Bawendi, M. G. Transport properties of annealed CdSe colloidal nanocrystal solids. *J. Appl. Phys.* **2002**, *92*, 7498.
(18) Jarosz, M. V.; Stott, N. E.; Drndic, M.; Morgan, N. Y.; Kastner, M. A.; Bawendi, M. G. Observation of bimolecular carrier recombination dynamics in close-packed films of colloidal CdSe nanocrystals. *J. Phys. Chem. B* **2003**, *107*, 12585.
(19) Porter, V. J.; Geyer, S.; Halpert, J. E.; Kastner, M. A.; Bawendi, M. G. Photoconduction in annealed and chemically treated CdSe/ZnS inorganic nanocrystal films. *J. Phys. Chem. C* **2008**, *112*, 2308.
(20) Leatherdale, C. A.; Kagan, C. R.; Morgan, N. Y.; Empedocles, S. A.; Kastner, M. A.; Bawendi, M. G. Photoconductivity in CdSe quantum dot solids. *Phys. Rev. B* **2000**, *62*, 2669.
(21) Jarosz, M. V.; Porter, V. J.; Fisher, B. R.; Kastner, M. A.; Bawendi, M. G. Photoconductivity studies of treated CdSe quantum dot films exhibiting increased exciton ionization efficiency. *Phys. Rev. B* **2004**, *70*, 195327.
(22) Fischbein, M. D.; Drndic, M. CdSe nanocrystal quantum-dot memory. *Appl. Phys. Lett.* **2005**, *86*, 193106.
(23) Fischbein, M. D.; Drndic, M. Nanogaps by direct lithography for high-resolution imaging and electronic characterization of nanostructures. *Appl. Phys. Lett.* **2006**, *88*, 063116.
(24) Bube, R. H. *Photoconductivity of Solids*; John Wiley & Sons, Inc.: New York, 1960.
(25) Crooker, S. A.; Barrick, T.; Hollingsworth, J. A.; Klimov, V. I. Multiple temperature regimes of radiative decay in CdSe nanocrystal quantum dots: Intrinsic limits to the dark-exciton lifetime. *Appl. Phys. Lett.* **2003**, *82*, 2793.

NL9024209